tained over macroscopic film thicknesses and large surface areas by vapor deposition of a single molecular species on an amorphous substrate. Inducing the non-centrosymmetric order by using selective hydrogen bonding to the substrate and between the molecules leads to a much better molecular ordering than with the technique described by Cai et al.,[13] which requires control of the molecular beam direction relative to the substrate. The present technique does not require a well-defined molecular beam, and is also much simpler and faster than the synthetic methods used by Ulman[7] and Marks and Ratner[18] or for LB films.

It is important to note that the alignment in our films is critically dependent on the ability of these molecules to selectively hydrogen bond to the surface, in order to begin the alignment process, and selectively hydrogen bond to itself in a unidirectional fashion in order to maintain the alignment over a large thickness. We have carried out preliminary experiments with molecules that only posses hydrogen bond acceptors and, therefore, can form hydrogen bonds to the substrate surface, but which lack hydrogen bond donors thus eliminating the possibility of intra-molecular hydrogen bonding, and have shown that only very thin films (of the order of a few monolayers thickness) with polar ordering perpendicular to the substrate surface can be grown. As the films grow thicker, we see that the ordering cannot be maintained.

In conclusion, we have shown a simple and efficient new method to produce supramolecular self-assembled thin films with well-defined polar ordering perpendicular to the substrate surface. The resulting films are homogenous over a large area, and a regular, deterministic molecular ordering can be maintained over a large thickness of the order of 1 μm. The fact that the films were grown on amorphous glass substrates circumvents the need for surface epitaxy. The quality of the films and the simplicity of the fabrication method make this novel technique very attractive for the fabrication of nonlinear optical waveguides for frequency conversion or electro-optic modulation. Despite the relatively low nonlinearity ($d_{111} = 5$ pm V^{-1}) that has been obtained in this first demonstration, the high degree of molecular ordering and the fact that the films consist of only one component make them potentially very interesting when compared to present candidates for organic electro-optic modulators, poled polymers. The higher degree of order and tighter molecular packing in our films should also lead to a better photostability when compared to amorphous systems with embedded chromophores.

A further detailed investigation of the mechanism that leads to the molecular ordering and an optimization of the growth conditions should lead to a new generation of organic waveguides for frequency conversion and electro-optic modulation.

Experimental.

BITINPH was purchased from Opto-Organics Industrial Research Limited and purified by recrystallization from ethanol. The amorphous glass substrates were cleaned by immersing them in an ultrasonic bath of acetone for 5 min and then in an ethanol bath for 5 min. The substrates were then immersed in a piranha solution (H_2SO_4:30 % H_2O_2, 70:30 vol./vol.) and left in it for 1 h at 80 °C (warning: piranha solution reacts violently with organic materials), they were then rinsed with deionized water and dried under vacuum at a temperature of 100 °C for 1 h. Thin films of BITINPH were grown by evaporation of the material, which was placed in a molybdenum boat and heated in a vacuum chamber that was kept at 10^{-6} torr vacuum.

Received: May 28, 2003
Final version: August 3, 2003

[1] C. Boshard, K. Suter, P. Pretre, J. Hulliger, M. Florsheim, P. Kaatz, P. Günter, *Organic Nonlinear Optical Materials*, Gordon & Breach, Amsterdam **1995**.
[2] F. Kajzar, J. D. Swalen, *Organic Thin Films for Waveguiding Nonlinear Optics*, Gordon & Breach, Amsterdam **1996**.
[3] G. M. Whitsides, J. P. Mathias, C. T. Seto, *Science* **1991**, *254*, 1312.
[4] L. V. Interrante, L. A. Casper, A. B. Ellis, *Materials Chemistry of Organic Monolayer and Multilayer Thin Films*, American Chemical Society, Washington, DC **1995**.
[5] R. H. Tredgold, *Order in Thin Organic Films*, Cambridge University Press, Cambridge **1994**.
[6] S. Miyata, H. S. Nalwa, *Organic Electroluminescent Materials and Devices*, Gordon & Breach, Amsterdam **1997**.
[7] A. Ulman, *Chem. Rev.* **1996**, *96*, 1533.
[8] S. R. Forrest, *Chem. Rev.* **1997**, *97*, 1793.
[9] R. Schlesser, T. Dietrich, Z. Sitar, F. Gitmans, A. Kündig, L. Eng, B. Münch, P. Günter, *J. Appl. Phys.* **1995**, *78*, 4943.
[10] M. Mobus, N. Karl, T. Kobayashi, *J. Cryst. Growth* **1992**, *116*, 495.
[11] C. D. Englund, G. E. Collins, T. J. Schuerlein, N. R. Armstrong, *Langmuir* **1994**, *10*, 2748.
[12] E. I. Haskal, F. F. So, P. E. Burrows, S. R. Forrest, *Appl. Phys. Lett.* **1992**, *60*, 3223.
[13] C. Cai, B. Müller, J. Weckesser, J. V. Barth, Y. Tao, M. M. Bösch, A. Kündig, C. Boshard, I. Biagio, P. Günter, *Adv. Mater.* **1999**, *11*, 750.
[14] C. Serbutoviez, C. Bosshard, G. Knöpfle, P. Wyss, P. Pretre, P. Günter, K. Schenk, E. Solari, G. Chapuis, *Chem. Mater.* **1995**, *7*, 1198.
[15] A. Rodger, B. Norden, *Circular Dichroism and Linear Dichroism*, Oxford University Press, Oxford **1997**.
[16] L. V. Natarajan, F. M. Stein, R. E. Blankeship, R. Chang, *Chem. Phys. Lett.* **1983**, *95*, 525.
[17] H. E. Kaatz, G. Sceller, M. T. Putvinski, M. L. Schilling, W. L. Wilson, C. E. D. Chidsey, *Science* **1991**, *254*, 1485.
[18] T. J. Marks, M. A. Ratner, *Angew. Chem. Int. Ed. Engl.* **1995**, *34*, 155.
[19] D. Li, B. I. Swanson, J. M. Robinson, M. A. Hoffbauer, *J. Am. Chem. Soc.* **1993**, *115*, 6975.
[20] D. A. Kleinman, *Phys. Rev.* **1962**, *126*, 1977.
[21] A. Facchetti, M. E. van der Boom, A. Abbotto, L, Beverina, T. J. Marks, G. A. Pagani, *Langmuir* **2001**, *17*, 5939.

An Electrospun Poly(vinylidene fluoride) Nanofibrous Membrane and Its Battery Applications

By *Sung Won Choi*, *Seong Mu Jo*,* *Wha Seop Lee*, and *Yong-Rok Kim*

Polymer electrolytes using perfluoropolymers, such as poly[(vinylidene fluoride)-*co*-hexafluoropropylene] (P(VdF-HFP)), as host polymers have been widely studied because they are known to be chemically and mechanically stable.[1,2]

[*] Dr. S. M. Jo, Dr. W. S. Lee
Polymer Hybrid Research Center
Korea Institute of Science and Technology
PO Box 131, Cheongryang, Seoul (Republic of Korea)
E-mail: smjo@kistmail.kist.re.kr
S. W. Choi, Dr. Y.-R. Kim
Department of Chemistry, Yonsei University
134, Sinchon-dong, Seodaemun-gu, Seoul (Republic of Korea)

 DOI: 10.1002/adma.200304617

ADVANCED MATERIALS

Gel polymer electrolytes are usually prepared by film-casting a homogeneous polymers solution dissolved in an electrolyte solution.[3,4] The mixing ratio of polymer to electrolyte solution can be easily controlled. Polymer gels encapsulate the electrolyte solution in the polymer hosts and at room temperature generally show high ionic conductivity of 1×10^{-3} S/cm or more.[5] All the processes must be performed in a moisture-free environment since lithium salts in an electrolyte solution are highly sensitive to moisture. However, the soft morphology of the gels is often unsuitable for high-speed processing in the manufacture of lithium polymer batteries. The flow properties of these electrolytes at high temperature can also lead to internal short circuits.[6] Therefore, gel polymer electrolytes are not suitable for commercial fabrication of lithium polymer batteries.

Highly crystalline PVdF homopolymer may be applied as a polymer electrolyte to overcome the mentioned disadvantages.[7,8] However, PVdF-based gel polymer electrolyte shows low ionic conductivity and electrochemical stability because the crystalline part of PVdF hinders the migration of Li^+ ions. The resulting lithium polymer battery also shows low charge/discharge capacity and poor *C*-rate value.[9]

The phase inversion method is a well-known technique for preparing nanoporous membranes with high porosity, large surface area, and excellent mechanical properties. A nanoporous polymer matrix was prepared by casting a polymer solution and evaporating the non-solvent and solvent in turn.[10,11] The polymer electrolyte was prepared using the activation method by impregnating the nanoporous matrix with the electrolyte solution. Outstanding work using the phase inversion and activation method was performed by Telecordia (formally Bellcore).[12] In their work, P(VdF-HFP) with lower crystallinity was used as the polymer matrix instead of PVdF.[13,14] These polymer electrolytes simultaneously show good electrochemical and mechanical properties. However, residual solvent or non-solvent cannot be easily removed, affecting electrochemical properties such as the electrochemical stability and safety of lithium polymer batteries.[15] Furthermore, commercial Li ion batteries using this polymer matrix as a separator suffer from low rate capability of only about 50 % of the designed capacity at high discharge rate (*C*/1 rate).

The porous polymer matrix from Telecordia or commercial polyolefin separators generally show pore sizes of tens of nanometers. However, the ionic conductivity of PVdF-based polymer electrolytes increases as the pore size of the porous polymer matrix increases from the nanometer to the micrometer range. Finally, the rate capability of a cell with this polymer electrolyte increases dramatically.[16,17]

The immersion precipitation method is applied to prepare this microporous structure. The activation of a PVdF microporous membrane with electrolyte solutions gives rise to multiphase systems that result in an amorphous swollen gel, crystalline strands, and cavities filled with the solution (liquid phase). The amount of electrolyte uptake, the membrane's porosity, pore size, interconnectivity, the conductivity of the neat electrolyte, the thickness of the membrane, and the extent to which the electrolyte wets the pore walls of the membrane are important factors in determining the ionic conductivity of this film.[18,19] These porous polymer electrolytes still maintain mechanical integrity, show good wettability for liquid electrolyte, and form a stable interface between electrode and electrolyte. Therefore, microporous polymer electrolytes are generally expected to have fast ion mobility, high ionic conductivity, low bulk impedance, and high rate capability. These characteristics render them more suitable for cells with high power density.

A microporous polymer matrix can be also prepared by electrospinning the polymer solution. Electrospinning is known to be a novel and efficient fabrication tool for preparing fibrous polymer membranes with fiber diameters ranging from several micrometers down to tens of nanometers.

An electrospun nanofibrous membrane has high porosity, pore size of a few tens of nanometers to a few micrometers, interconnected open pore structure, high permeability of gas, and large surface area per unit mass. Electrospinning technology recently came into the spotlight for applications in fields such as filters, biomedical materials, fiber mats in reinforcing components, clothing providing protection from electromagnetic waves, sensor engineering, radioactive radiation, and electronic devices.[20–22]

In electrospinning a polymer solution, a high voltage is applied to a very thin tip of a nozzle connected to a syringe or a reservoir containing a polymer solution. When the voltage is increased to just below the threshold value, a droplet of polymer solution at the tip is deformed into a conical shape known as a Taylor cone. In this case, charge or dipole orientation will be formed at the interface between air and the droplet of polymer solution. When the applied electric voltage overcomes the surface tension of the polymer solution, one or more jets of polymer solution are ejected from the tip of the nozzle and fly towards the collector. Eventually, a fibrous membrane of nanofibers forms on the surface of the collector. The nanofibers are deposited at a rate of several meters per second.[23] The solvent is easily evaporated and the polymer jet is elongated when the fiber flies toward the collector.[24] Solvent evaporation occurs on the time scale of several milliseconds.[25] The rapid evaporation of solvent during electrospinning of the polymer solution is related to phase separation in the polymer jet. Phase separation influences the fiber diameter and surface morphology.[26,27]

In this study, an electrospun PVdF nanofibrous membrane was investigated as a microporous polymer matrix for a polymer electrolyte. The polymer electrolyte was prepared by soaking the PVdF nanofibrous membrane in an electrolytic solution with 1 M $LiPF_6$-EC/DMC (1:1, wt./wt.), where EC is ethylene carbonate and DMC dimethyl carbonate. Its electrochemical properties, such as ionic conductivity, interfacial resistance, and electrochemical stability were then measured. Owing to the micropore structure and high porosity of the polymer matrix, the electrolyte solution may be easily inserted into and tightly held in the pores of the polymer matrix. The polymer electrolyte is expected to show good electro-

chemical properties such as high ionic conductivity, sufficient electrochemical stability, and low interfacial resistance. Thus, this polymer electrolyte will maintain sufficient mechanical strength due to its three-dimensional network structure with fully interconnected fibers.

The nanofibrous membrane was prepared by electrospinning PVdF (Kynar 761) solution in an acetone/*N*,*N*-dimethylacetamide (DMAc; 3:7 wt./wt.) mixture. When a strong electric field was applied, PVdF polymer jets were sufficiently elongated when the fiber flew toward the collector because of the relatively slow evaporation caused by the high boiling point of DMAc.

The resulting fibrous membrane (Fig. 1) consists of fibers with a smooth surface, a well-controlled average diameter of 250 nm, as determined by scanning electron micrography (SEM), and mean pore size of about 0.65 μm, as determined

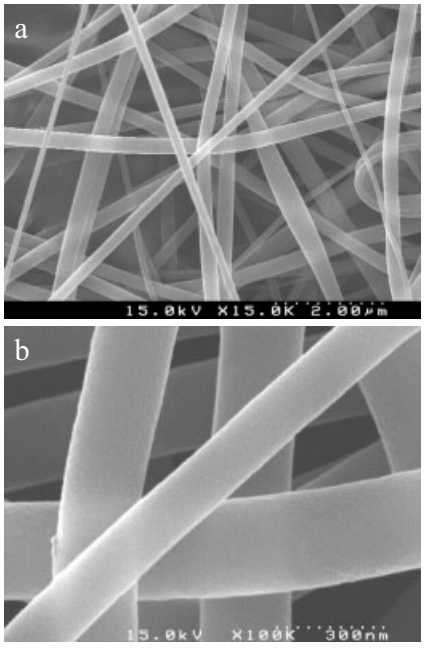

Fig. 1. SEM images of PVdF nanofibrous membrane obtained by electrospinning of PVdF solution in acetone/DMAc (3:7, wt./wt.): a) ×15 000, b) ×100 000.

using a capillary flow porometer. Electrospun PVdF nanofibrous membranes show a fully interconnected pore structure with narrow pore size distribution and apparent porosity of about 83 %.[28] In the case of electrospun fibrous membrane, the porosity calculated by the uptake of butanol may result in some error because of large openings formed by the interstices between fibers on the surface layer of the fibrous membrane.

The melting temperature and melting enthalpy of PVdF powder and electrospun PVdF nanofibrous membrane were determined by differential scanning calorimetry (DSC). As shown in Table 1, PVdF nanofibrous membrane shows an almost identical melting point and crystallinity to the PVdF powder received. However, PVdF polymer electrolyte shows lower crystallinity than PVdF powder and PVdF nanofibrous

Table 1. Thermodynamic properties of PVdF powder, electrospun PVdF nanofibrous membrane, and PVDF nanofibrous polymer electrolyte.

Sample	Melting point T_m [°C]	Melting enthalpy ΔH_m [J/g]	Crystallinity X_c [a] [%]
PVdF powder	167	46.8	44.7
PVdF nanofibrous membrane	166	46.0	43.9
PVdF polymer electrolyte:			
Ethylene carbonate	6.34	35.1	–
Gelled PVdF	94.4	8.66	8.27
Partially swelled PVdF	123	4.26	4.07

[a] $X_c = (\Delta H_m^{sample}/\Delta H_m^*) \times 100$, $\Delta H_m^* = 104.7$ J/g

membrane. Although PVdF is swelled by the electrolyte solution, electrospun PVdF nanofiber-based membrane maintains its three-dimensional network structure. It also shows sufficient mechanical strength for use as the matrix in polymer electrolyte.

In wide-angle X-ray scattering (WAXS) diffraction patterns of a nanofibrous membrane and nanofibrous polymer electrolyte (not shown here), the PVdF nanofibrous membrane showed similar peak patterns (two major peaks at 2θ = 18.3°, 20.5° and two minor peaks at 2θ = 36.4°, 56.9°) to the typical WAXS peaks of PVdF powder with form II (α type). This indicated that there was no serious change of crystal structure caused by electrospinning in a strong electric field.[29] However, after soaking the nanofibrous membrane in the electrolyte solution, the PVdF nanofibers in the fibrous membrane were partially swollen because of the penetration of electrolyte solution. Thus, their peaks either disappeared or broadened because of partial collapse of the PVdF crystal structure.

From these results, the nanofibrous polymer electrolyte is assumed to consist of solid polymer phase with partially swollen PVdF fibers, a gel phase formed on the fiber surface by swelling, and a liquid phase of pores filled with the electrolyte solution.

After soaking in electrolyte solution, the nanofibrous polymer electrolyte showed self-standing membrane characteristics with some mechanical strength. Solid polymer phase with partially swollen PVdF fibers still supports the membrane structure and exhibits mechanical strength.

On the other hand, the electrochemical properties of this nanofibrous polymer electrolyte will be influenced by the gel and liquid phases. Nanofibrous membrane shows good wettability for electrolyte solution due to its large specific surface area. Therefore, the nanofibrous membrane shows excellent ability to hold electrolyte solution.

The determination of the uptake of electrolyte solution still includes some error due to the large openings formed by the interstices between fibers in the surface layer of the fibrous membrane. Even so, the amount of electrolyte solution soaked up by the fibrous membranes was about 260 wt.-%, indicating high solvent retention ability of the electrospun nanofibrous membrane. For comparison, that of the polyolefin separator (Celgard, thickness 20 μm, porosity 40 %) in the same electrolyte solution was only about 130 %. This is due to

ADVANCED MATERIALS

the polyolefin separator's lower affinity for liquid electrolyte and lower porosity.

Figure 2 shows the ionic conductivity and impedance change of this polymer electrolyte. The ionic conductivity of the electrospun fibrous membrane electrolyte was measured from the alternating current (AC) impedance spectra of the SS/nanofi-

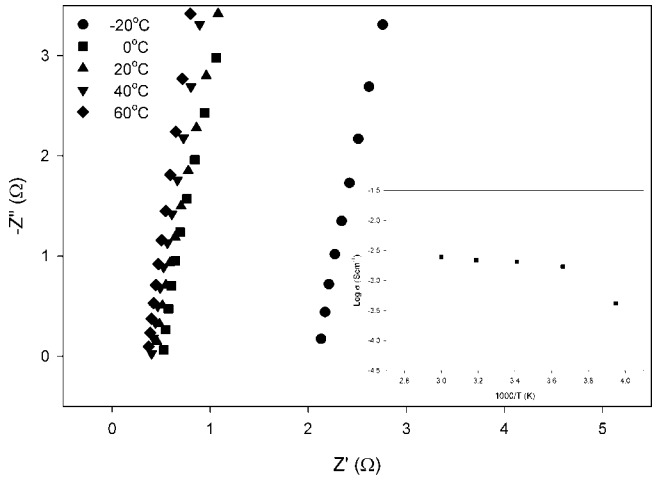

Fig. 2. Ionic conductivities of PVdF nanofibrous polymer electrolyte at several temperatures. The inset shows ionic conductivity, σ, plotted as a function of inverse temperature.

brous polymer electrolyte/SS (SS = stainless steel) over the range of –20 to 60 Ω. The nanofibrous polymer electrolyte exhibits high ionic conductivity of about 1.7×10^{-3} S/cm at 0 °C. Most gel polymer electrolytes show high ionic conductivity of more than 1×10^{-3} S/cm at room temperature. However, the polymer gel electrolyte with PVdF homopolymer generally shows very low ionic conductivity due to its high crystallinity and the crystallization of electrolyte solution at low temperature. Although PVdF homopolymer with high crystallinity was used as the nanofibrous polymer matrix, the nanofibrous polymer electrolyte shows high ionic conductivity, which is sufficient for use in a lithium polymer battery.

PVdF nanofibrous membrane shows a fully interconnected pore structure with high porosity. It also shows excellent wettability by the electrolyte solution, owing to the high surface area of the nanofiber and good affinity of PVdF for the electrolyte solution.

Lithium ion conduction is more dependent on the liquid-like electrolyte phase in the pores than on the swollen gel phase in the polymer electrolytes with microporous structure.[30] Lithium ions can easily move through the pore structure of the nanofibrous polymer electrolyte. Therefore, the high ionic conduction in the PVdF nanofibrous polymer electrolyte mainly depends on the electrolyte solution phase with higher conductivity in the micropore structure, in addition to the minor contribution of a swollen polymer phase with lower conductivity. However, the swollen phase on the surface of the nanofiber not only suppresses the leakage of electrolyte solution from electrospun nanofibrous polymer electrolyte but also contributes to the ionic conductivity, especially at low temperature.

Ionic conductivity increased with increasing temperature and decreased at temperatures below 0 °C (Fig. 2). This is due to the crystallization of ethylene carbonate (EC) in electrolyte solution, as shown in Table 1. Crystallized ethylene carbonate is known to greatly hinder the migration of lithium ions, decreasing the ionic conductivity at low temperature. When the polymer matrix is sufficiently swelled by the electrolyte solution, a drastic decrease of ionic conductivity due to solidification of solvent may be greatly suppressed.[11] PVdF nanofibrous membrane shows excellent wettability by electrolyte solution due to the high surface area of the nanofiber and good affinity of PVdF for the electrolyte solution. Therefore, crystallization of solvent in the nanofibrous polymer electrolyte may be sufficiently reduced. The resulting fibrous polymer electrolyte exhibited high ionic conductivity of about 1.7×10^{-3} S/cm at 0 °C.

The interfacial resistance between lithium and the nanofibrous polymer electrolyte was confirmed from the impedance data of a symmetric Li/PVdF nanofibrous polymer electrolyte/Li cell. Figure 3 shows the Cole–Cole plots for the symmetric cell. The semicircle is attributed to the parallel combination of resistance (R_{film}) and capacitance (C_{dl}) asso-

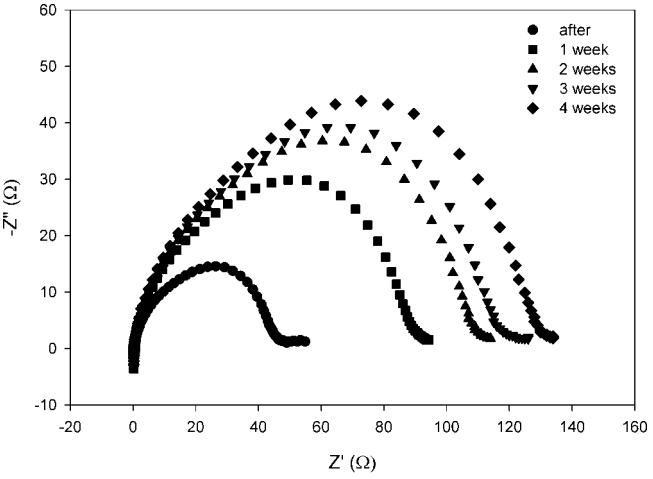

Fig. 3. Cole–Cole plots of the PVdF-based polymer electrolyte using electrospun PVdF nanofibrous membrane.

ciated with the passivation layer between the nanofibrous polymer electrolyte and lithium electrode. The resistance (R_{bulk}) of the nanofibrous polymer electrolyte was an almost constant value. On the other hand, the resistance due to the passivation layer continuously increased with time. However, the interfacial resistance due to the passivation layer between lithium and the nanofibrous polymer electrolyte was very small. In the case of a prototype cell composed of $LiCoO_2$/PVdF nanofibrous polymer electrolyte/graphite, it was confirmed that a compact and dense passivation layer was formed after the charge/discharge test (not shown here). Based on this, the PVdF nanofibrous polymer electrolyte was assumed

to maintain a stable interface with the lithium electrode during the charge/discharge process.

The electrochemical stability window of the nanofibrous polymer electrolyte was measured using linear sweep voltammetry between 2.0 and 5.0 V. Figure 4 shows the electrochemical stability of the nanofibrous polymer electrolyte containing 1 M $LiPF_6$-EC/DMC (1:1, wt./wt.). Generally, the

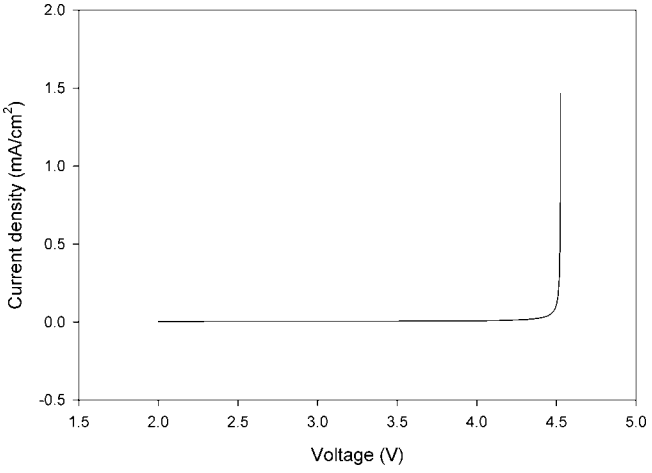

Fig. 4. Linear sweep voltammogram of the PVdF nanofibrous polymer electrolyte.

oxidation peak for free liquid electrolyte is observed at about 3.9 V. As shown in Figure 4, the nanofibrous electrolyte showed good oxidation stability of the polymer electrolyte on the anode up to 4.5 V. The presence of the host polymer causes an increase in the anodic limit voltage to 0.6 V with respect to the solution itself. This higher resistance is caused by the resulting gel phase in the activated membrane.[31] The PVdF nanofibrous membrane showed excellent wettability of the electrolyte solution due to the high surface area of nanofiber and good affinity of PVdF for the electrolyte solution. This gel phase formed by the swelling of PVdF fibers is thought to cause an enhancement of the electrochemical stability window. Therefore, nanofibrous polymer electrolyte is expected to be stable within the operating voltage region of the lithium polymer battery.

In summary, the electrospun nanofibrous membrane had high porosity, large surface area, fully interconnected pore structure, and sufficient mechanical strength. A nanofibrous polymer electrolyte using this membrane showed excellent physical and electrochemical properties. Therefore, the electrospun nanofibrous membrane is considered to be a good microporous polymer matrix of polymer electrolytes for high-performance lithium polymer batteries.

Experimental

Poly(vinylidene fluoride) (PVdF) is a commercial product (Kynar Flex 761, Elf Atochem) with average molecular weight (M_n) of 5.5×10^5 g/mol. A known amount of PVdF powder was homogeneously dissolved in an acetone/*N*,*N*-dimethylacetamide (DMAc) solvent mixture. The polymer solution was charged in a syringe. The silver-coated needle of the syringe was connected to a high-voltage power supply (Bertan, Model 230). Then, a stainless steel plate for collection of electrospun fiber was grounded. After this, the feed rate of polymer solution through the syringe was controlled with a syringe infusion/withdrawal pump (KD Scientific, Model 220). A fibrous membrane with a thickness of 30 μm was deposited on the collector plate by electrospinning of PVdF solution under high voltage of 10–15 kV.

The electrospun nanofiber-based membrane was dried under vacuum at 80 °C for 12 h. Polymer electrolyte was then prepared by soaking the electrospun fibrous membrane in the electrolyte solution: 1 M $LiPF_6$ in ethylene carbonate (EC)/dimethyl carbonate (DMC) (1:1, wt./wt.) mixture.

Under vacuum, SEM (S-4200 scanning microscope, Hitachi Co.) was used to observe the fibrous membranes. The electrospun PVdF nanofiber-based membrane was gold-coated prior to SEM measurements.

Mean pore diameter and pore size distributions were measured using a capillary flow porometer (PMI, ver. 7.0). Here, mean pore diameter refers to "mean flow pore diameter". Air pressure was applied to one side of a fluid-saturated membrane. Airflow through the membrane was recorded at various differential pressures. Pore size was calculated from the "wet" and "dry" flow curves. A perfluoropolyether (1,1,2,3,3,3-hexafluoropropene, oxidized, polymerized) was used as a wetting solvent in this experiment.

The WAXS diffraction patterns of the electrospun PVdF nanofibrous membrane and its polymer electrolyte were obtained using an X-ray diffractometer (MAC science, MX018) with Cu Kα radiation. The scanning rate was 1°/min, and the samples were scanned in the range 5°–70°.

The thermal properties of PVdF powder and the electrospun nanofiber-based membrane were investigated using differential scanning calorimetry (Perkin-Elmer Co., DSC-7) under N_2 atmosphere. The heating rate was 10 °C/min, and the samples were scanned in the range –50 to 200 °C.

Ionic conductivity was measured using the impedance technique over the frequency range 0.1 Hz–100 kHz and temperature range from –10 °C to 60 °C using an IM6e (Zahner Co.). The conductivity cell consisted of two stainless steel blocking electrodes.

The change of interfacial resistance between lithium metal and the polymer electrolyte was investigated at room temperature for 28 days using the impedance analyzer. The measuring cell consisted of two lithium non-blocking electrodes.

Linear sweep voltammetry was used to determine the electrochemical stability of the polymer electrolyte. The measurement was carried out with a three-electrode electrochemical cell consisting of a nickel working electrode, a lithium reference, and a counterelectrode. The measurement was performed at room temperature and the scan rate was 1 mV/s.

Received: November 14, 2002
Final version: September 15, 2003

[1] Z. Jiang, B. Carroll, K. M. Abraham, *Electrochim. Acta* **1997**, *42*, 2667.
[2] H. S. Choe, J. Giaccai, M. Alamgir, K. M. Abraham, *Electrochim. Acta* **1995**, *40*, 2293.
[3] H. Akashi, K. Tanaka, K. Sekai, *J. Electrochem. Soc.* **1998**, *145*, 881.
[4] C. S. Kim, S. M. Oh, *Electrochim. Acta* **2001**, *46*, 1323.
[5] a) A. S. Gozdz, C. N. Schmutz, J. M. Tarascon, P. C. Warren, *US Patent 5 540 091*, **1996**. b) W. Huang, J. R. Akridge, *Mater. Res. Soc. Symp. Proc.* **1999**, *548*, 325. c) A. M. Christie, L. Christie, C. A. Vincent, *J. Power Sources* **1998**, *74*, 77.
[6] Z. Jiang, B. Carroll, K. M. Abraham, *Electrochim. Acta* **1997**, *42*, 2667.
[7] S. Abbrent, J. Plestil, D. Hlavata, J. Lindgren, J. Tegenfeldt, Å. Wendsjö, *Polymer* **2001**, *42*, 1407.
[8] M. Morita, M. Ishikawa, Y. Matsuda, in *Lithium Ion Batteries* (Eds: M. Wakihara, O. Yamamoto), Wiley-VCH, Weinheim **1998**, Ch. 7.
[9] K. M. Kim, N.-G. Park, K. S. Ryu, S. H. Chang, *Polymer* **2002**, *43*, 3951.
[10] H. Kataoka, Y. Saito, T. Sakai, E. Quartarone, P. Mustarelli, *J. Phys. Chem. B* **2000**, *104*, 11 460.
[11] Y. Saito, H. Kataoka, A. M. Stephan, *Macromolecules* **2001**, *34*, 6955.
[12] A. S. Gozdz, C. N. Schmutz, J. M. Tarascon, P. C. Warren, *US Patent 5 418 091*, **1995**.
[13] K. M. Abraham, Z. Jiang, B. Carroll, *Chem. Mater.* **1997**, *9*, 1978.
[14] Y. Saito, H. Kataoka, C. Capiglia, H. Yamamoto, *J. Phys. Chem. B* **2000**, *104*, 2189.
[15] a) F. Boudin, X. Andrieu, C. Jehoulet, I. I. Olsen, *J. Power Sources* **1999**, *81–82*, 804. b) X. Andrieu, C. Jehoulet, F. Boudin, I. I. Olsen, in *Proc. of the 38th Power Sources Conf.*, Cherry Hill, NY, June **1998**, p. 266.
[16] H. Wang, H. Huang, S. L. Wunder, *J. Electrochem. Soc.* **2000**, *147*, 2853.
[17] J. Y. Song, Y. Y. Wang, C. C. Wan, *J. Power Sources* **1999**, *77*, 183.
[18] K. M. Abraham, *Electrochim. Acta* **1993**, *38*, 28.

ADVANCED MATERIALS

[19] A. du Pasquier, P. C. Warren, D. Culver, A. S. Gozdz, G. G. Amatucci, J. M. Tarascon, *Solid State Ionics* **2000**, *135*, 249.
[20] P. P. Tsai, H. S. Gibson, P. Gibson, *J. Electrostatics* **2002**, *54*, 333.
[21] H. Yoshimoto, Y. M. Shin, H. Terai, J. P. Vacanti, *Biomaterials* **2003**, *24*, 2077.
[22] X. Wang, C. Drew, S.-H. Lee, K. J. Senecal, J. Kumar, L. A. Samuelson, *Nano Lett.* **2002**, *2*, 1273.
[23] K. K. Baumgarten, *J. Colloid Interface Sci.* **1971**, *36*, 71.
[24] M. Bognitzki, W. Czado. T. Frese, A. Schaper, M. Hellwig, M. Steinhart, A. Greiner, J. H. Wendorff, *Adv. Mater.* **2001**, *13*, 70.
[25] H. Fong, D. H. Reneker, *J. Polym. Sci., Part B: Polym. Phys.* **1999**, *37*, 3488.
[26] S. Koombhongse, W. Liu, D. H. Reneker, *J. Polym. Sci., Part B: Polym. Phys.* **2001**, *39*, 2598.
[27] H. Fong, I. Chun, D. H. Reneker, *Polymer* **1999**, *40*, 4585.
[28] J.-Y. Lai, F.-C. Lin, C.-C. Wang, D.-M. Wang, *J. Membrane Sci.* **1996**, *118*, 49.
[29] M. Tazaki, R. Wada, M. Okabe, T. Homma, *J. Appl. Polym. Sci.* **1997**, *65*, 1517.
[30] H. Huang, S. L. Wunder, *J. Electrochem. Soc.* **2001**, *148*, A279.
[31] J. M. Tarascon, A. S. Gozdz, C. N. Schmutz, F. Shukoki, P. C. Warren, *Solid state Ionics* **1996**, *49*, 86.

Synthesis of Aragonite Nanofilament Networks by Mesoscale Self-Assembly and Transformation in Reverse Microemulsions**

By *Mei Li*, *Benedicte Lebeau*, and *Stephen Mann**

The integration of nanosized components into functional materials and devices requires new technologies that provide reproducible processing and assembly of nanostructures across extended length scales. Current chemical approaches usually involve the controlled organization of preformed nanoparticles into relatively simple close-packed superstructures by solvent evaporation,[1,2] molecular cross-linking,[3,4] or programmed recognition,[5–7] or through the use of patterned substrates.[8,9] In contrast, other studies have demonstrated the potential of direct methods, in which synthesis and self-assembly are coupled in situ to produce higher-order nanoparticle-based structures.[10] These reactions are undertaken in complex media, such as water-in-oil microemulsions or aqueous solutions containing anionic polyelectrolytes, and result in the spontaneous organization of incipient inorganic–organic nanoparticles by mesoscale assembly and transformation of stable or metastable building blocks.[11] In the latter case, remarkable complex higher-order architectures such as twisted bundles, cones, and helicoids, often with self-similar structure, are produced by aggregation and subsequent crystallization of surfactant–polymer-stabilized amorphous nanoparticles.[12–18]

[*] Prof. S. Mann, Dr. M. Li
School of Chemistry, University of Bristol
Bristol BS8 1TS (UK)
E-mail: s.mann@bris.ac.uk
Dr. B. Lebeau
Laboratoire de Matériaux Minéraux
CNRS UMR 7016, ENSCMu, UHA
3 rue Alfred Werner, F-68093 Mulhouse Cedex (France)

[**] We thank Dr. Julian Eastoe for the gift of surfactant-stabilized amorphous calcium carbonate particles, Dr. Alex Kulak for technical expertise, and EPSRC for financial support to ML.

A common feature of these organized materials is the spontaneous embedding of structures over multiple length scales, which arises as an emergent property of the system that is not directly related to the smallest building block but dependent on how these units evolve in time and space. For example, the slow transformation of surfactant-stabilized amorphous nanoparticles within colloidal aggregates can be strongly coupled with rearrangements of surface-adsorbed organic molecules such that the organization and morphology of the resulting nanocrystals are modulated according to the length scale of the growing structure. Although the mechanistic details require further elucidation (see Coelfen and Mann for details),[11] the degree of cooperativity associated with these mesoscale disorder–order transformations is strongly influenced by the surface charge and degree of hydration of the inorganic phase and surfactant headgroups. In microemulsion-based reactions, these can be controlled, respectively, by changes in the reactant molar ratio[10,12] and the number of water droplets per amorphous nanoparticle (n),[18] for a constant $[H_2O]$/[surfactant] molar ratio (w) equal to 10. In the latter case, changes in the value of n produced a range of organized hybrid surfactant–vaterite ($CaCO_3$) nanostructures associated with the water-induced crystallization of alkylbenzenesulfonate-coated amorphous calcium carbonate (ACC) nanoparticles in water-in-isooctane sodium bis(2-ethylhexyl)sulfosuccinate (NaAOT) microemulsions. Here, we extend these studies to a detailed investigation of the reaction system at an increased w value of around 20. Surprisingly, no vaterite nanostructures are formed under these conditions. Instead, remarkable doughnut-shaped micrometer-sized particles with mesoporous sponge-like internal structures consisting of interlinked aragonite nanofilaments are produced by the surfactant-mediated transformation and crystallization of the ACC precursor nanoparticles. Although nanofilament networks and mesoporous phases are rare for calcium carbonates, such materials could have important uses as catalyst supports, fillers, and pigments, as well as in the design of novel biomimetic scaffolds for targeted drug release and tissue engineering.[19]

Addition of dry samples of surfactant-stabilized ACC nanoparticles to NaAOT microemulsions prepared in isooctane at $w = 20$ and $n = 680$ produced transparent solutions that became slightly turbid within 30 min and cloudy after 2 h, followed by the gradual appearance of a white precipitate at the bottom of the test-tube. Powder X-ray diffraction analysis (d-spacings (hkl indices): 0.336 (111), 0.287 (002), 0.269 (012), 0.248 (200), 0.234 (130), 0.197 (221), 0.187 (202) nm) and Fourier transform infrared (FTIR) spectroscopy (vibrational bands; 700, 712, 864, 1082, and 1476 cm^{-1}) indicated that the precipitate collected after 5 h was aragonite. In addition, FTIR spectra of the as-prepared samples showed bands corresponding to ester C=O (1735 cm^{-1}), ester C=O, and S=O (1219 cm^{-1}), C=C aromatic (1595 and 1467 cm^{-1}), C–H methyl (2960, 2874 cm^{-1}), C–H methylene (2931, 2861 cm^{-1}), and O=S=O (1169 cm^{-1}) vibrations, indicating that significant amounts of alkylbenzenesulfonate and NaAOT were associated with the precipitate. This was confirmed by energy dis-

  DOI: 10.1002/adma.200305589